Improved convolutional neural network-based bearing fault diagnosis using multi-phase motor current signals

Hai Dang Huu[1], Ngoc-My Bui[2], Van-Phuc Hoang[3], Thang Bui Quy[3], Yen Hoang Thi[4]
[1]Institute of Electronics, Academy of Military Science and Technology, Hanoi, Vietnam
[2]Department of Training, Academy of Military Science and Technology, Hanoi, Vietnam
[3]Institute of System Integration, Le Quy Don Technical University, Hanoi, Vietnam
[4]Faculty of Radio-Electronic Engineering, Le Quy Don Technical University, Hanoi, Vietnam

Article Info

ABSTRACT

Diagnosing bearing faults of the induction motor is crucial for the maintenance of rotating electrical machines. Numerous methods have been developed and published for monitoring and classifying these faults using sensor data such as vibration, audio, and current signals. Ideally, the current phases are balanced; however, faults disrupt this symmetry, causing each phase to reveal unique diagnostic details. Consequently, studies that rely on a single phase of the current signal may not capture all fault-related characteristics. Research on motor bearing fault diagnosis using two current phases typically extracts features from each phase separately, applying machine learning to classify the faults. Currently, no approach has been proposed to extract features from both phases simultaneously. Furthermore, the proposed solutions have only been published with noise-free data. To address these challenges, this paper introduces an enhanced solution that improves the accuracy of motor bearing fault classification based on an improved convolutional neural network that processes current signals from two phases simultaneously. Experimental results demonstrate that the proposed method significantly outperforms traditional approaches, particularly in scenarios where the sample signals are noise-adding signals. Fault classification accuracy of the proposed improved convolutional neural network (MI-CNN) about 95.12% with noise-adding signals at the signal-to-noise ratio of 20 dB.

Corresponding Author:

Van-Phuc Hoang
Institute of System Integration, Le Quy Don Technical University
236 Hoang Quoc Viet Road, Bac Tu Liem District, Hanoi, Vietnam
Email: phuchv@lqdtu.edu.vn

1. INTRODUCTION

Electrical machines in general and induction motors in particular are crucial in various industries. Due to continuous operation, these motors experience significant electrical and mechanical pressure, making them susceptible to failure. Failures can result from the motor itself, operating conditions or installation errors, leading to reduced motor lifespan and increased production losses if not detected early. Consequently, techniques have been developed to identify and assess failures, enhancing the reliability and availability of electric motors [1]. Motor failures commonly occur in components such as bearings, stators, rotors, among others [2]. Among these components, bearing failures are the most prevalent, accounting for over 40% of motor failures. According to research by Sing and Al Kazzaz [3], bearing failure is the primary cause of motor malfunctions. Bearings are essential for the durable and stable operation of motors, so when they are

damaged, whether through broken rollers or chipped inner or outer rings, it directly impacts motor performance, causing improper operation and loud noises. The various types of damage in induction motors are illustrated in Figure 1 [4].
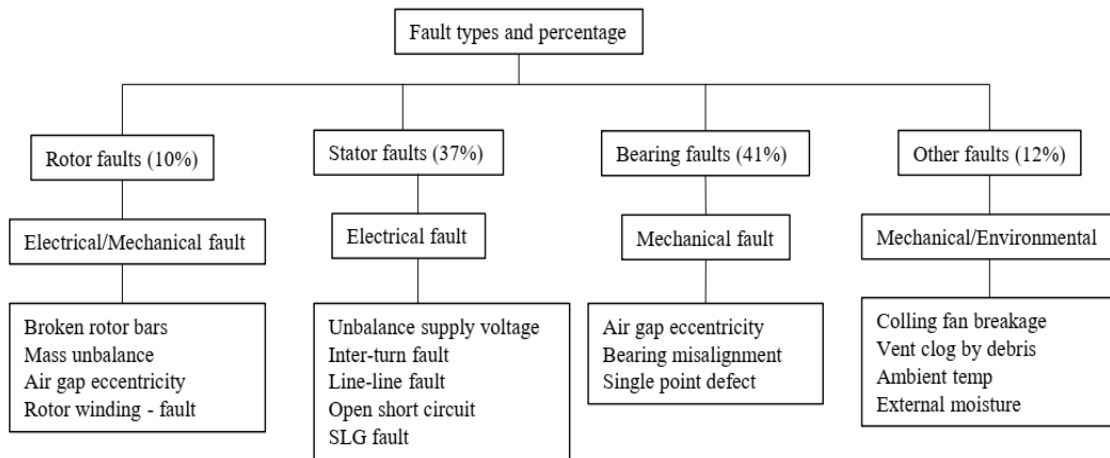

Figure 1. Classification of common faults in induction motors [4]

Figure 2 describes rolling-element bearing structure and faults, in which Figure 2(a) illustrates the structure of a typical bearing and the damage that can occur to its outer and inner rings is illustrated in Figure 2(b) and Figure 2(c) respectively [5]. A bearing consists of two rings, called the inner and outer rings, with a set of rolling balls positioned on rolling surfaces that rotate around these rings. Continuous stress on the bearings can lead to fatigue, typically manifesting as damage to the inner or outer ring. This damage results in small pieces breaking off the bearing, a phenomenon known as flaking or cracking [6], which in turn causes unstable bearing operation. Several factors can contribute to bearing failure, including the quality of the bearing itself, operating in environments prone to oxidation or chemical corrosion and insufficient periodic maintenance. Such conditions not only impair the smooth operation but also increase friction, reducing lifetime of the bearing. To prevent production interruptions caused by engine failures, extend operating time and optimize investment efficiency, fault detection and condition monitoring are essential. Fault detection helps prevent unexpected interruptions and mitigates the risk of serious damage to the entire powertrain, while condition monitoring reduces maintenance costs and enhances engine reliability.

(a)   (b)   (c)
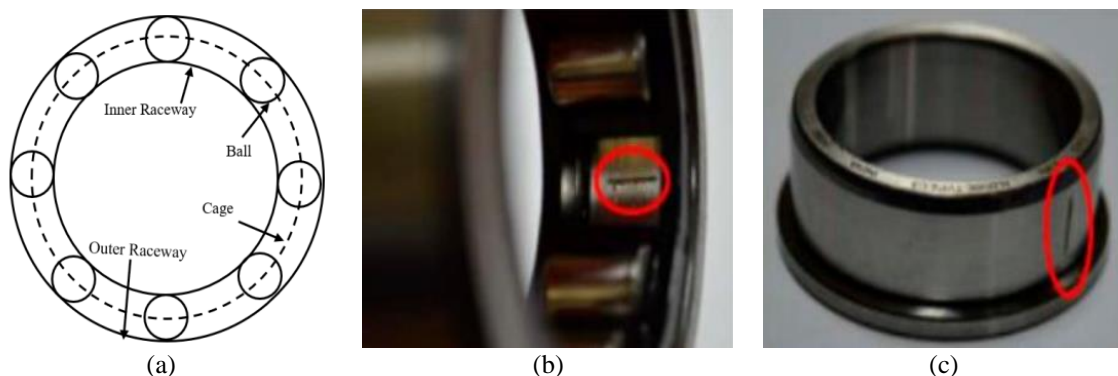
Figure 2. Rolling-element bearing structure and faults (a) structure of a rolling-element bearing,
(b) outer race fault, and (c) inner race fault [5]

Up to now, various methods have been developed and applied for detecting and diagnosing motor bearing faults, including sound and vibration analysis [7], electromagnetic field monitoring [8] and motor current signal analysis (MCSA) [9]. Researchers have also investigated fault diagnosis techniques based on other motor physical quantities, including rotor position, rotor speed, torque, power capacity, and

temperature, in addition to these signal-based approaches [10]. Among these, vibration and sound signal analysis are widely used for detecting motor bearing faults. However, these methods require the use of expensive sensors and the proper placement and installation of these sensors can be challenging due to limited construction space. Additionally, the presence of noise from surrounding devices can interfere with the accuracy of sound measurements, leading to potential misdiagnoses when using sound sensors to detect bearing faults. Compared to vibration and sound monitoring, MCSA method has gained significant attention due to several key advantages. Firstly, MCSA does not require additional sensors, as it utilizes the existing current signal from the motor controller, which reduces both costs and system complexity. Additionally, this method allows for the remote monitoring of multiple motors from a single location by analyzing the current signal supplied to each motor [11]. Furthermore, MCSA is less affected by ambient noise since it relies on current signals for diagnosing bearing faults, making it a more reliable option in noisy environments.

Typically, bearing fault diagnosis using current data with traditional methods involves two main steps: fault feature extraction and fault classification. fast Fourier transform (FFT) [12], discrete wavelet transform (DWT) [12], empirical mode decomposition (EMD) [13], local mean decomposition (LMD) [14] and variational mode decomposition (VMD) [15] are commonly used feature extraction techniques. For fault classification, popular machine learning algorithms include support vector machine (SVM) [16], back-propagation neural network [17], Bayesian classifier [18], k-nearest neighbor (k-NN) [19], random forest (RF) [20] and classification and regression tree (CART) [21]. The accuracy of bearing fault diagnosis using the above approaches depends on the manual selection of extracted signal features and training of the machine learning classifier. To overcome this, deep learning-based motor bearing fault diagnosis methods, typically convolutional neural network (CNN) models, are widely applied [22]–[24]. These are published works on motor bearing fault diagnosis based on a single phase of motor current signal.

In theory, when a two-phase electric motor experiences a fault, the current in the two phases becomes asymmetrical, meaning they each carry distinct information about the system fault. Therefore, the accuracy of the above solutions is not high due to missing symptoms of bearing failure. Both phases of the current signal must be used for bearing fault diagnosis in order to improve diagnostic accuracy and decrease missed detections. To date, there are only a few studies exploring the use of two-phase motor current signals for diagnosing bearing faults. Published works on diagnosing motor bearing faults based on two phases of current signals only extract features of each phase individually [5], [25]. This is not suitable for diagnosing motor bearing faults using multiple phases of current signals simultaneously. Thus, this paper proposes a new solution, termed multi-input CNN (MI-CNN), to overcome the current disadvantages of the previous methods for detecting bearing failures in a multi-phase motor. In this method, feature maps from both phases of the current signal are extracted concurrently through two branches of the proposed MI-CNN model. These extracted features are then integrated during the fusion stage and subsequently classified by a softmax classifier. Simulations conducted in various noisy environments demonstrate that the proposed method achieves superior diagnostic accuracy compared to existing solutions, including those based on deep learning and machine learning with multi-sensor signals. The subsequent sections of this article provide a thorough explanation of the recommended bearing fault diagnosis method, the experimental dataset, validation, and discussion.

2. PROPOSED METHOD
2.1. Basic CNN model structure for diagnosing electric motor bearing damage

The basic CNN model structure for diagnosing electric motor bearing faults is depicted in Figure 3. It comprises several key components: an input layer (a grayscale image block of dimensions L1×L2), five convolutional blocks, three pairs of nonlinear and fully connected layers, a softmax layer, and an output layer. The first four convolutional blocks each consist of four layers: a convolutional layer, a normalization layer, a nonlinear activation layer, and a pooling layer. The fifth convolutional block includes a convolutional layer and a normalization layer. Padding is applied at the convolutional layers with a stride of 1×1 after each multiplication, ensuring that no information is lost and that the image dimensions remain unchanged.

The first fully connected layer in the basic CNN model contains 200 neurons, followed by the second fully connected layer with 100 neurons and the final fully connected layer with 3 neurons. These three neurons correspond to the bearing condition labels: 0, 1, and 2, representing a no-fault bearing, an inner race break bearing, and an outer race failure bearing, respectively. This basic CNN model, as depicted in Figure 3, offers advantages such as low model complexity, rapid training time, and efficient image classification. However, it is limited by its ability to diagnose motor bearing faults using only one phase of the current signal, leading to lower accuracy and requiring a huge amount of iterations for the model to converge, particularly in noisy environments. To diagnose motor bearing faults using both phases of the motor current simultaneously, enhancements to the basic CNN model are necessary.

2.2. Structure of the proposed MI-CNN model for electric motor bearing fault diagnosis

The proposed MI-CNN model, illustrated in Figure 4, is composed of four stages: data collection, feature extraction, feature fusion, and classification. The data collection and feature extraction stage consist of two branches: the left and right branches, which are used to collect and extract features using signals from Phase 1 and Phase 2 of the motor current, respectively. Each branch follows an identical structure. Signals from Phase 1 and Phase 2 are first converted into grayscale images of dimensions L1×L2. These images serve as the input to the CNN model, which comprises five convolutional normalization rectified linear unit max-pooling (CNRM) blocks and a fully connected layer (FC1). The first four CNRM blocks share the same structure as the convolutional blocks of the basic CNN model described in section 2.1. The fifth CNRM block includes a convolutional layer, a normalization layer, and a nonlinear activation layer. The output from the first fully connected layer (FC1) is then fed into the feature fusion block, where features extracted from the two phases of the current signal are combined, allowing the MI-CNN model to simultaneously extract features from two phases. The number of neurons of this layer is concatenated by neurons of the FC1 layer of the two branches. The feature classification stage consists of two pairs of rectified linear unit (ReLU) and fully connected layers, followed by a softmax layer and an output layer. This stage classifies the input image into one of three categories, labeled 0, 1, or 2, corresponding to different bearing fault conditions, based on the probabilities calculated by the softmax layer, similar to the basic CNN model. The next section of the paper will present the dataset for experimental verification of the proposed model effectiveness, the scenario, and experimental method.
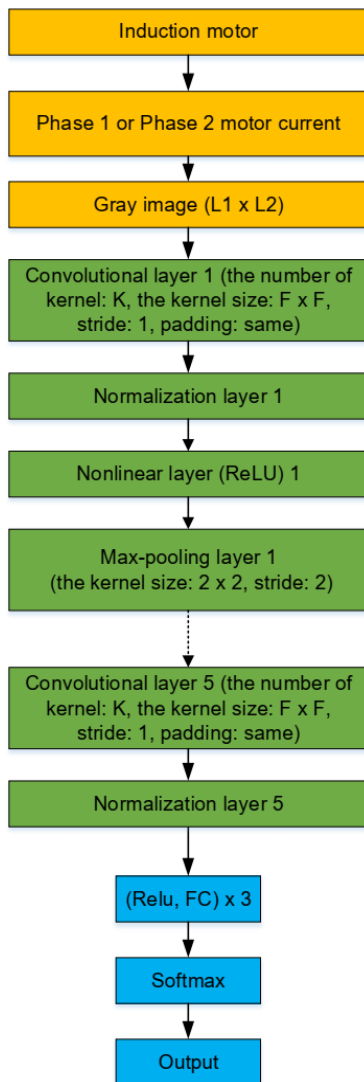
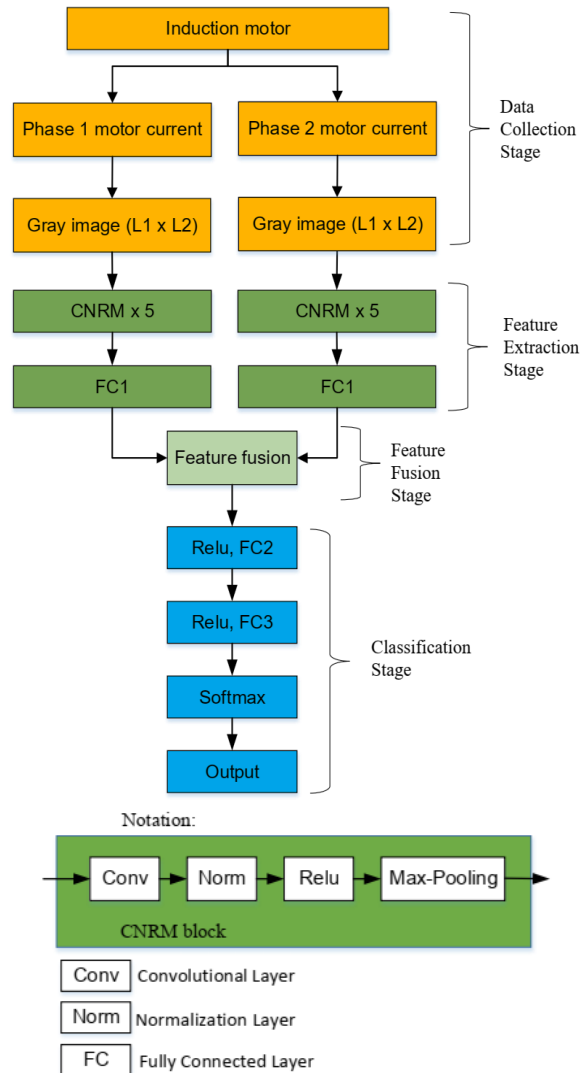Figure 3. Basic CNN model structure for diagnosing electric motor bearing damage

Figure 4. Diagram of the proposed MI-CNN model structure for diagnosing electric motor bearing faults

3. EXPERIMENTAL DATA AND METHOD

3.1. Experimental data

We use the bearing dataset provided by Paderborn University [26] to simulate the proposed MI-CNN model, which is a laboratory-measured dataset and has been used by many research groups to test the proposed bearing fault diagnosis solution ([5], [22], [23], [25]). The published dataset includes measurements of various motor parameters corresponding to 32 bearing codes of type 6203, with specifications as described in Table 1. These bearings are categorized into naturally damaged, artificially damaged, and undamaged groups, consisting of 6 undamaged bearings (K001-K006), 12 bearings with outer ring faults (KA01, KA03-KA09, KA15, KA16, KA22, KA30), 11 bearings with inner ring faults (KI01, KI03-KI05, KI07, KI08, KI14, KI16-KI18, KI21), and 3 bearings with both inner and outer ring faults (KB23, KB24, KB27).

Table 1. Bearing parameters of type 6203

Parameters	Value
Bearing type	Deep groove ball
Bearing designation	6203
Diameter of inner race	24.00 mm
Diameter of outer race	33.10 mm
Pitch circle diameter	29.05 mm
Rolling element diameter	6.75 mm
Number of rolling elements	8
Nominal pressure angle	0^0

Figure 5 displays the schematic diagram of the test stand that measures the parameters of the signals that describe the motor's physical quantities. It is made up of the following parts: an electric motor (1), a torque measuring shaft (2), a bearing test module (3), a flywheel (4), and a load motor (5). Bearings with different failure modes are mounted in the bearing test module to generate simulation data. The motor (1) is a 425 W permanent magnet synchronous motor (PMSM) with a rated torque of T=1.35 Nm, a rated rotor shaft speed of n=3000 rpm, a rated current of I=2.3 A and the number of pole pairs of p=4. It is operated by a frequency converter (KEB Combivert 07F5E 1D-2B0A) with a cut-off frequency of 16 kHz. This motor has 4 operating states corresponding to different values of rotor shaft rotation speed (S), load torque (M), radial force acting on bearings (F). Table 2 indicates four working conditions of the motor. The load motor (5) is Siemens-Motor 1FT7062-1AF70-1DG1. In this paper, we use two phases of the current signals of 15 bearing codes are depicted in Table 3, corresponding to the working state B of the motor in Table 2 to do experiment. Given a sampling frequency of 64 kHz and a measurement duration of 4 seconds, each current signal measurement comprises 256.000 data points (64.000 samples/second×4 seconds). For each bearing code, 20 measurements are conducted, resulting in a total of 5.120.000 data points per bearing code (256.000×20). Since each bearing label in Table 3 contains 5 bearing codes, the total number of data points per bearing label amounts to 25.600.000 (5.120.000×5).
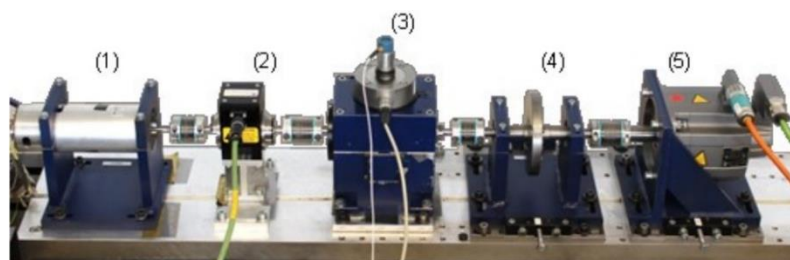

Figure 5. Test stand for measuring engine parameters [24]

Table 2. Engine working conditions

Operating state	S (RPM)	M (Nm)	F (N)
A	1500	0.1	1000
B	900	0.7	1000
C	1500	0.7	400
D	1500	0.7	1000

Table 3. The bearing codes used for experiment

Bearing condition	Class	Label	Bearing code
Non-faulty (N)	0	K0	K001, K002, K003, K004, K005
Outer race damage (O)	1	KA	KA04, KA15, KA16, KA22, KA30
Inner race damage (I)	2	KI	KI04, KI14, KI16, KI18, KI21

3.2. Experimental method

The data points of both phases of the motor current signal when operating with labels K0, KA, and KI in Table 3 are divided into grayscale images, each with a size of L1 L2 pixels. Therefore, the number of images corresponding to the labels K0, KA and KI in Table 3 is 25.600.000/(L1 L2) images. The allocation of input images to the MI-CNN model is performed randomly as follows: 80% of the images are assigned for training and the remaining 20% are reserved for testing and evaluation. The parameters of the MI-CNN model for the experiment are listed in Table 4. The mini-batch size is chosen to be 128. If the value of the mini-batch size is too small, the number of iterations will increase, leading to the state of the model gradually moving from underfitting to optimal and then overfitting. On the contrary, if the mini-batch size is too large, buffer memory is needed to store the training data. Furthermore, to verify the effectiveness and reliability of the recommended model, Gaussian noise was added to the signals used for testing. In this paper, the proposed method is tested by changing the coefficients L1, L2 (L1 L2=40 40, 60 60, 80 80, and 100 100); K (1, 5, 10, 20, and 30), F (3 3, 5 5, 7 7, 9 9, and 11 11); and varying the value of = 0.001, 0.01, and 0.1 on many signals with different signal-to-noise ratios, including signal-to-noise ratio (SNR)=-10, -5, 0, 5, 10, 15, and 20 dB to select the optimal parameter set of the model based on the criteria of fault classification accuracy and classification time of an image used for model testing. After selecting the optimal parameter set, we compare the electric motor bearing fault classification accuracy of the proposed solution using the proposed MI-CNN model with the basic CNN model and compare the results of the proposed solution with other works using 2-phase data such as [5] and [25] using the same dataset, executed on the same hardware platform (Intel (R) Core i7 2.9 GHz CPU; 8 GB RAM) using MATLAB software to highlight the effectiveness of the proposed method.

Table 4. Parameters of the proposed MI-CNN

Parameter	Value
Input image size	L1×L2
Minibatch Size	128
InitialLearnRate	α
LearnRateDropFactor	0.1
ValidationPatience	5
L2Regularization	1e-10
Epoch	10
The number of kernels/the kernel size per convolutional layers	K/F
Optimizer	Adam

4. EXPERIMENTAL RESULTS AND DISCUSSION

4.1. Evaluation of the fault identification accuracy of the proposed MI-CNN model when changing the initial training rate

In this experiment, we selected the proposed MI-CNN model with a random set of values: L1 × L2 (40×40), K (5), F (7×7) and varied the learning rate α (0.001, 0.01, and 0.1). The input data consisted of two-phase motor current signals with added Gaussian noise at different SNR values. Figure 6 shows the classification accuracy of motor bearing faults using the proposed MI-CNN model with two-phase motor current signals at an SNR of 20 dB, tested at three different initial learning rates with $\alpha = 0.1$ in Figure 6(a), $\alpha = 0.01$ in Figure 6(b), and $\alpha = 0.001$ in Figure 6(c). The experiment was repeated using different SNR values and the results of the bearing breakdown diagnosis accuracy and the time to classify a single image for varying initial learning rates are presented in Table 5 and Table 6, respectively.
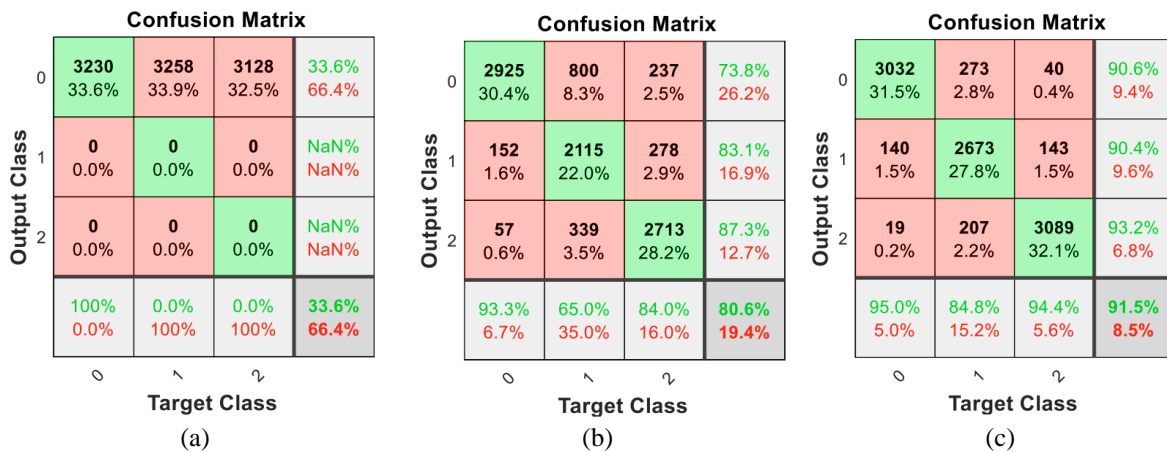
Table 5 demonstrates that with the proposed MI-CNN, the more the training rate is reduced, the more the fault classification accuracy increases, and the highest accuracy is achieved at the rate of 0.001 among the three rate values used for experiments at all experimental signals with different SNR values. This aligns with theoretical expectations, where a learning rate that is too high may cause the model to converge too quickly to a suboptimal solution, while a learning rate that is too low can cause the training process to stall. However, according to Table 6, decreasing the training rate will result in the longer time needed to classify a single input image during testing and model evaluation. To balance between fault classification accuracy and execution time, we choose $\alpha = 0.001$ for the proposed MI-CNN model.

Table 5. Fault classification accuracy with different initial learning rates

The initial learning rates	The fault classification accuracy (%) with the noise-adding signal at the different SNR						
	20 dB	15 dB	10 dB	5 dB	0 dB	-5 dB	-10 dB
0.1	33.60	33.55	33.50	33.50	33.50	33.45	33.30
0.01	80.60	76.83	67.73	54.60	44.68	38.30	33.50
0.001	91.50	84.40	71.30	59.44	50.20	46.80	46.70

Table 6. Classification time per image with different initial learning rates

The initial learning rates	Number of images to be classified	The total weight (with L1×L2=40×40, K=5, F=7×7)	Time to classify 1 image (ms)
0.1	9600	59243	3.11±0.3
0.01	9600	59243	3.15±0.3
0.001	9600	59243	3.19±0.3

Figure 6. The fault classification accuracy of the proposed MI-CNN model with different initial training rates, experiment with the 20 dB SNR signal (a) $\alpha = 0.1$, (b) $\alpha = 0.01$, and (c) $\alpha = 0.001$

4.2. Evaluation of the fault identification accuracy of the proposed MI-CNN model when varying numbers of kernels

In this experiment, we selected the proposed MI-CNN model with a random set of values: L1×L2 (60×60), F (5×5), α (0.001) and varied the K values of 1, 5, 10, 20, and 30. The input data consisted of two-phase motor current signals with added Gaussian noise at different SNR values. Figure 7 illustrates the classification accuracy of motor bearing faults for five different kernel quantities per convolutional layer using the proposed MI-CNN model using two-phase motor current signals at an SNR of 15 dB with K=1, 5, 10, 20, 30 in Figures 7(a) to 7(e) respectively. The experiment was repeated using other SNR values and the results of classification accuracy and the time taken to classify a single image with varying kernel quantities are presented in Tables 7 and 8, respectively.

According to Table 7, the proposed MI-CNN model with 1 kernel per convolutional layer has the lowest classification accuracy. The accuracy is significantly improved if we use larger kernel number per convolutional layer such as 5, 10, 20 and the accuracy is maximized with a kernel number of 30 in all experimental signals. This aligns with theory, which suggests that increasing the number of kernels allows the CNN model to learn deeper signal features. Therefore, the fault classification accuracy is significantly increased. However, as shown in Table 8, increasing the number of kernels in each convolutional layer also leads to a larger number of weights (44683 for the model with 1 kernel versus 523203 for the model with 30 kernels), resulting in a longer classification time per image (2.58 ± 0.2 ms versus 6.79 ± 0.6 ms). Tables 7 and 8 show that using 5 kernels per layer yielded only a slightly lower classification accuracy compared to using 30 kernels (87.5% versus 89.9% with an SNR of 15 dB). However, the classification time per image for the model with 5 kernels per convolutional layer was significantly reduced compared to the model with 30 kernels, due to the much lower total number of weights (64203 versus 523203). To balance between fault classification accuracy and execution time, we select K=5 among the five kernel values used for experimentation for the proposed MI-CNN model.

Figure 7. Fault classification accuracy of the MI-CNN model with varying numbers of kernels, experiment with the 15 dB SNR signal (a) K=1, (b) K=5, (c) K=10, (d) K=20, and (e) K=30

Table 7. Fault classification accuracy with varying numbers of kernels

Number of kernels	Fault classification accuracy (%) with the noise-adding signal at the different SNR						
	20 dB	15 dB	10 dB	5 dB	0 dB	-5 dB	-10 dB
1	70.30	65.20	59.69	51.24	46.68	44.27	43.66
5	91.79	87.50	75.41	71.30	50.91	48.24	46.40
10	92.32	89.59	81.00	77.24	53.35	48.88	47.50
20	92.85	89.80	83.35	80.16	54.68	49.52	48.40
30	93.59	89.90	85.86	82.54	58.62	50.33	49.60

Table 8. Classification time per image with varying numbers of kernels

Number of kernels/convolutional layers	Number of images to be classified	Total weight (L1×L2=60×60, F=5×5)	Time to classify one image (ms)
1	4267	44683	2.58±0.2
5	4267	64203	3.35±0.3
10	4267	97603	3.68±0.3
20	4267	322403	5.82±0.5
30	4267	523203	6.79±0.6

4.3. Evaluation of the fault identification accuracy of the MI-CNN model when varying kernel sizes

In this experiment, we selected the proposed MI-CNN model with the following parameters: L1×L2 (80×80), K (10), α (0.001) and varied the kernel sizes F of 3×3, 5×5, 7×7, 9×9, and 11×11. The input data image consisted of two-phase motor current signals with added Gaussian noise at different SNR values. Figure 8 illustrates the classification accuracy of motor bearing faults using the enhanced CNN model with five different kernel sizes per convolutional layer, using two-phase motor current signals at an SNR of 10 dB with F=3×3, 5×5, 7×7,9×9, and 11×11 in Figures 8(a) to 8(e) respectively. The experiment was repeated with other SNR values, and the results for classification accuracy and the time to classify a single image with different kernel sizes are presented in Tables 9 and 10, respectively.

Tables 9 and 10 demonstrate that, with the proposed model, increasing the kernel size not only reduces the malfunction identification accuracy but also increases the total weight of the model, leading to an increase in the time required to classify an image in all experimental signals. According to Tables 9 and 10, we chose the kernel size in each convolutional layer as 3×3 for the suggested MI-CNN model to reach the highest accuracy and ensure the fastest image classification time compared to the remaining kernel sizes. This aligns with theory, which suggests that choosing a small kernel size will extract highly local features, detect small features, extract diverse features, be useful for the following layers, and share weights well.

Table 9. Fault classification accuracy with varying kernel sizes

Kernel size/ convolutional layers	Fault classification accuracy (%) with noise-adding signal at different SNR values						
	20 dB	15 dB	10 dB	5 dB	0 dB	-5 dB	-10 dB
3×3	95.72	91.12	87.60	73.34	62.35	57.92	52.16
5×5	94.72	88.89	86.70	72.28	60.23	56.28	51.21
7×7	93.51	85.30	80.80	70.10	59.20	55.78	50.87
9×9	91.14	84.48	79.10	68.82	58.90	54.32	50.33
11×11	89.35	82.23	75.90	66.47	57.57	53.66	48.90

Table 10. Classification time per image with varying kernel sizes

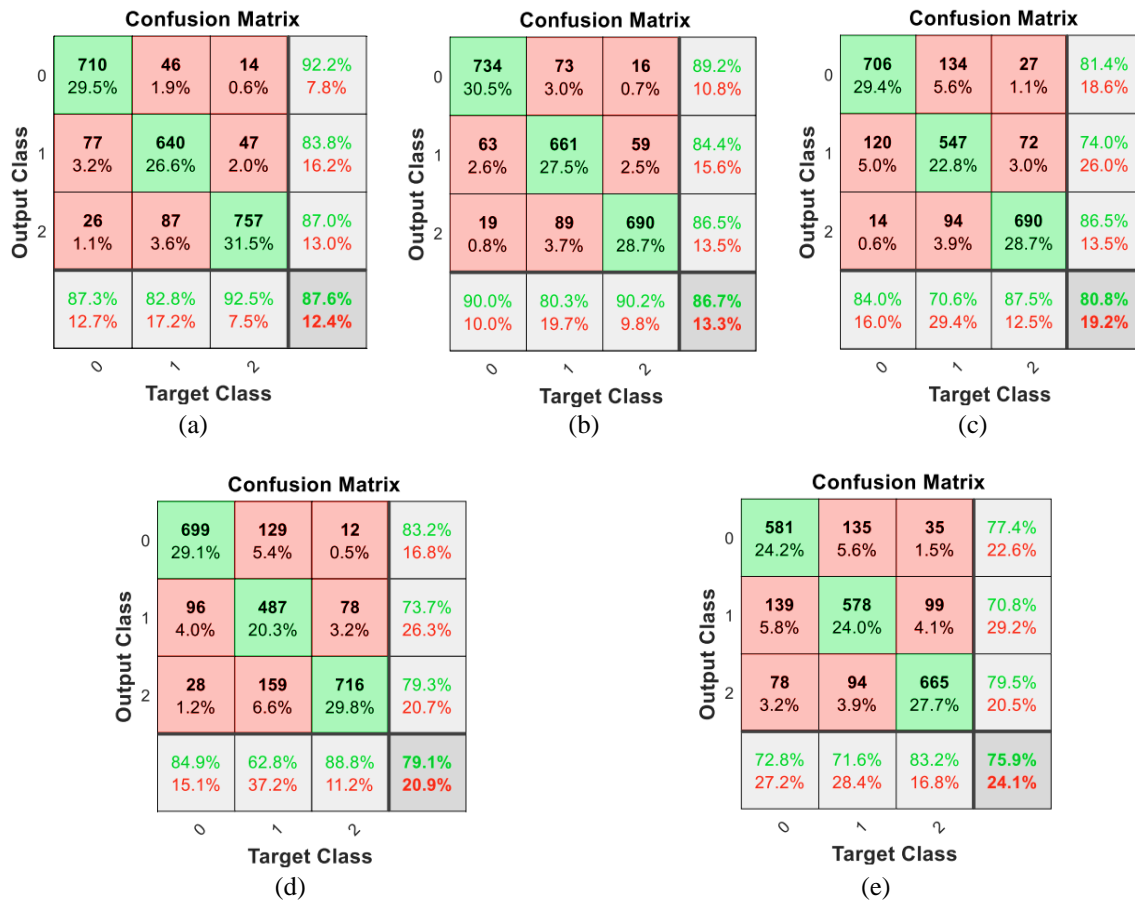| Kernel size/convolutional layers	Number of images to be classified	Total weight (with L1×L2=80×80, K=10)	Time to classify one image (ms)
3 × 3	2400	148483	3.64 ± 0.3
5 × 5	2400	161603	3.75 ± 0.3
7 × 7	2400	181283	3.92 ± 0.3
9 × 9	2400	207523	3.96 ± 0.5
11 × 11	2400	240323	3.99 ± 0.6

Figure 8. Fault classification accuracy of the proposed MI-CNN model with varying kernel sizes, evaluation with the 10 dB SNR signal (a) F=3×3, (b) 5×5, (c) F=7×7, (d) 9×9, and (e) F=11×11

4.4. Evaluation of the fault identification accuracy of the MI-CNN model when varying input data sizes

In this experiment, we selected the CNN model with F=11×11, K=1, α=0.001 and varying the L1×L2 values of 40×40, 60×60, 80×80, and 100×100 with input data consisting of two-phase motor current signals with added Gaussian noise at different SNR values. Figure 9 shows the classification accuracy of motor bearing faults for five different input data sizes using the proposed MI-CNN model using two-phase motor current signals at an SNR of 0 dB with L1×L2=40×40, 60×60, 80×80, and 100×100 in Figures 9(a) to 9(d) respectively. The experiment was repeated with other SNR values and the results for classification accuracy and the time to classify a single image with different input data sizes are presented in Tables 11 and 12, respectively.

4.5. Fault classification accuracy comparison of proposed MI-CNN model and basic CNN model

In this experiment, we used the proposed MI-CNN model with two-phase motor current signals and the basic CNN model with signals from phase 1 or phase 2. The parameters for the CNN model are detailed in Table 13. With an input image size of 80×80, each bearing code in Table 3 has 25.600.000/6400=4000 images, with 3200 images used for training and 800 images used for testing. Experiments were conducted with both models using data with and without Gaussian noise, at SNR levels of 20, 15, 10, 5, 0, -5, and -10 dB and compared the accuracy and classification time of the two models.
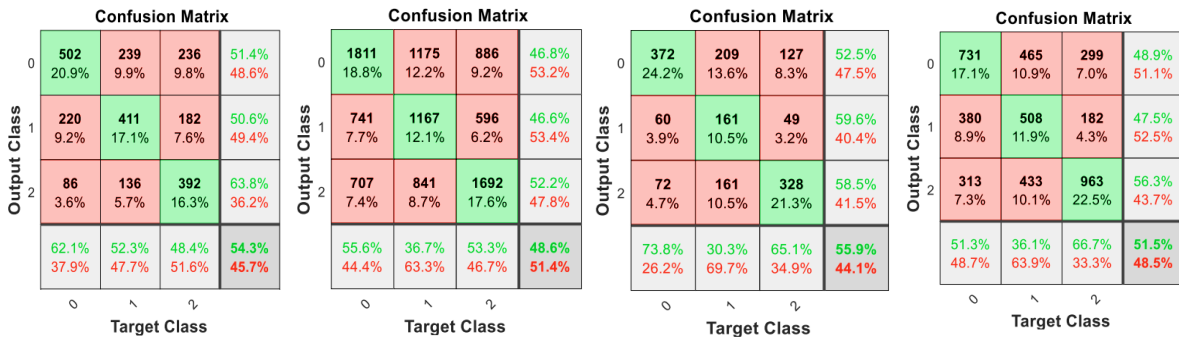

Figure 9. Fault classification accuracy of the proposed MI-CNN model with different input image sizes, experiment with the 0 dB SNR signal (a) L1×L2=40×40, (b) (b) L1×L2=60×60, (c) L1×L2=80×80, and (d) L1×L2=100×100

Table 11. Fault classification accuracy with varying input image sizes

Input image size	Fault classification accuracy (%) with noise-adding signal at different SNR values						
	20 dB	15 dB	10 dB	5 dB	0 dB	-5 dB	-10 dB
40 × 40	81.22	72.38	66.22	60.94	54.30	48.40	44.80
60 × 60	72.05	66.82	59.19	52.48	48.60	46.37	42.85
80 × 80	81.96	80.20	74.40	64.67	55.90	49.79	47.82
100 × 100	79.80	76.44	62.08	56.34	51.50	47.18	44.68

Table 12. Classification time per image with varying input image sizes

Input image size	Number of images to be classified	Total weight (with F=11 × 11, K=1)	Time to classify one image (ms)
40 × 40	9600	43643	1.23 ± 0.1
60 × 60	4267	45643	2.50 ± 0.2
80 × 80	2400	52043	3.40 ± 0.3
100 × 100	1536	56443	6.39 ± 0.6

Table 13. Parameters of proposed MI-CNN model

Parameter	Value	Parameter	Value
Input image size	80 × 80	L2Regularization	1e-10
Minibatch size	128	Epoch	10
InitialLearnRate	0.001	Number of kernels/Kernel size in convolutional layers	5/3 × 3
LearnRateDropFactor	0.1	Optimizer	Adam
ValidationPatience	5	Number of convolutional layers	5

The classification accuracy of the bearing faults for both models is summarized in Table 14. The accuracy curves for the models are presented in Figure 10. Table 14 demonstrates that the bearing fault diagnosis method using two phases of motor current signals simultaneously achieves significantly higher accuracy than the method using only one phase of current signal with the same model parameters for all experimental signals with different SNRs. The failure identification accuracy outstanding of the proposed MI-CNN model over the basic model is further demonstrated in signals with low SNR ratios. For example, with a signal having an SNR of 0 dB, the defect diagnosis accuracy of the MI-CNN model is 65.48% compared to 51.30% and 52.45% of the basic CNN model when using phase 1 and phase 2, respectively.
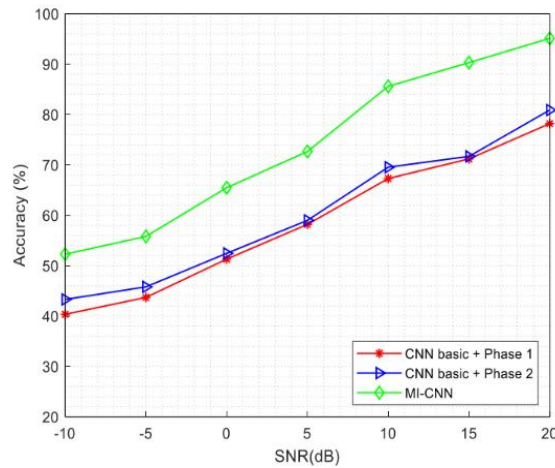
Figure 10. Comparison of fault classification accuracy between CNN models

Table 14. Comparison of fault classification accuracy and bearing fault classification time between the basic CNN model and the proposed MI-CNN model

| Method | Fault classification accuracy (%) with noise-adding signal at different SNR values | | | | | | | | Total weight | Time to classify one image (ms) |
	Noise-free	20 dB	15 dB	10 dB	5 dB	0 dB	-5 dB	-10 dB		
Basic CNN+Phase 1	91.02	78.20	71.20	67.30	58.20	51.30	43.70	40.35	46623	1.05 ± 0.1
Basic CNN+Phase 2	92.10	80.90	71.70	69.55	59.00	52.45	45.80	43.30	46623	1.05 ± 0.1
MI-CNN (this paper)	97.78	95.12	90.31	85.60	72.67	65.48	55.80	52.28	92843	3.43 ± 0.3

4.6. Fault classification accuracy comparison of proposed MI-CNN model with other methods using two-phase motor current signals

In this experiment, various methods utilizing two-phase motor current signals as simulation data were evaluated, including DWT and XGBoost machine method [5], deep learning and information fusion method [25] and the proposed MI-CNN solution. The dataset on bearing fault samples was used to compare the effectiveness of the methods listed in Table 3, with both noise-free signals and Gaussian noise at SNR levels of 20, 15, 10, 5, 0, -5, and -10 dB. Figure 11 shows the accuracy curves for bearing malfunction diagnosis corresponding to various techniques in noisy environments. Table 15 presents the accuracy of the various solutions with noise-free signals and signals with added Gaussian noise.

With the proposed MI-CNN model, during the process of extracting features, there is always additional information about failure between the two phases, helping the extracted features to be more diverse and informative. This leads to a significant improvement in the proposed MI-CNN model's fault classification accuracy. Indeed, Table 15 demonstrates that, with noise-adding signal, the motor bearing fault classification accuracy of the proposed MI-CNN model is higher than the published methods [5], [25] using two phases of motor current signals with the same experimental dataset and the same hardware platform, especially with signals with large SNR. For example, with a signal having an SNR of 10 dB, the failure diagnosis accuracy of the proposed MI-CNN model is 85.60% compared to 72.03% [25], 75.50% [25] and 72.38% [5].

Table 15 also presents that, with noise-free signals, the accuracy of the proposed method is higher than that of the IF+CNN [25] method (97.78% versus 96.13%) but slightly lower than that of the DWT and the XGBoost machine method [5] (97.78% versus 99.32%). Because the DWT and XGBoost machine method [5] uses the signal pre-processing techniques (applying the notch filter to remove 60 Hz signal). Additionally, the method in [5], extracts features for all four operational states of the motor listed in Table 2.

Therefore, the fault signatures are supplemented by various working conditions of the engine, making the fault diagnosis more accurate.

Figure 11 shows that, the accuracy of the proposed method is higher than other methods [5], [25]. Nevertheless, due to the lack of pre-processing techniques, the accuracy of the proposed method is only more outstanding than these methods for signals with high SNRs (20, 15, and 10 dB). Conversely, for signals with low SNRs (-10, -5, and 0 dB), the accuracy of the proposed MI-CNN model is not much better than that of remaining methods.
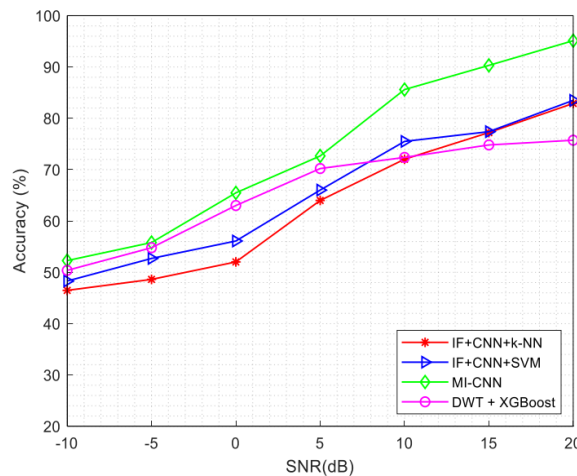
Figure 11. Comparison of fault classification accuracy between methods using two-phase current signals

Table 15. Comparison of fault classification accuracy among methods using two-phase motor current signals

Method	Fault classification accuracy (%) with noise-adding signal at different SNR values							
	Noise-free	20 dB	15 dB	10 dB	5 dB	0 dB	-5 dB	-10 dB
IF+CNN+k-NN [25]	96.13	82.9	77.22	72.03	64	52.02	48.62	46.48
IF+CNN+SVM [25]	96.13	83.5	77.4	75.5	66.02	56.1	52.7	48.3
DWT+XGBoost [5]	99.32	75.73	74.81	72.38	70.22	63.01	54.79	50.38
MI-CNN (this paper)	97.78	95.12	90.31	85.6	72.67	65.48	55.8	52.28

5. CONCLUSION

This paper proposes a new method to improve the accuracy of diagnosing electric motor bearing faults based on an improved CNN model called MI-CNN, which simultaneously uses both phases of the motor current signal. The published methods for diagnosing motor bearing faults using two phases of the motor current signal extract features of each signal phase individually. Therefore, the fault symptoms expressed in the asymmetry between phases when the motor fails are not extracted in the published methods. In contrast, our proposed method solves the problem of simultaneously extracting features in both phases of the motor current based on the proposed MI-CNN model. This makes the extracted features more diverse and more informative about the fault signatures, suitable for practical applications of diagnosing multi-phase electric motor bearing faults. Many experiments are conducted to select the optimal parameters of the proposed model. Then, we compare the bearing fault diagnosis accuracy of the recommended method with published methods. Using experimental signals with varying SNRs, the results demonstrate that the suggested approach outperforms published methods in terms of accuracy. Future research will consider testing the proposed MI-CNN model with different operational states of motors and with other types of motors. Additionally, the proposed method should be implemented with various signal pre-processing techniques for further accuracy enhancement.

REFERENCES

[1]   X. Liang, M. Z. Ali, and H. Zhang, "Induction motors fault diagnosis using finite element method: A review," *IEEE Transactions on Industry Applications*, vol. 56, no. 2, pp. 1205–1217, Mar. 2020, doi: 10.1109/TIA.2019.2958908.

[2]   C. P. Mboo and K. Hameyer, "Fault diagnosis of bearing damage by means of the linear discriminant analysis of stator current features from the frequency selection," *IEEE Transactions on Industry Applications*, vol. 52, no. 5, pp. 3861–3868, Sep. 2016, doi: 10.1109/tia.2016.2581139.

[3] G. K. Singh and S. Ahmed Saleh Al Kazzaz, "Induction machine drive condition monitoring and diagnostic research—a survey," *Electric Power Systems Research*, vol. 64, no. 2, pp. 145–158, Feb. 2003, doi: 10.1016/s0378-7796(02)00172-4.

[4] X. Liang and K. Edomwandekhoe, "Condition monitoring techniques for induction motors," in *2017 IEEE Industry Applications Society Annual Meeting*, Oct. 2017, pp. 1–10, doi: 10.1109/ias.2017.8101860.

[5] R. Nishat Toma and J.-M. Kim, "Bearing fault classification of induction motors using discrete wavelet transform and ensemble machine learning algorithms," *Applied Sciences*, vol. 10, no. 15, Jul. 2020, doi: 10.3390/app10155251.

[6] N. Mehala, "Condition monitoring and fault diagnosis of induction motor using motor current signature analysis," Ph.D. dissertation, Electrical Engineering Department, National Institute of Technology Kurukshetra, 2010.

[7] N. W. Nirwan and H. B. Ramani, "Condition monitoring and fault detection in roller bearing used in rolling mill by acoustic emission and vibration analysis," *Materials Today: Proceedings*, vol. 51, pp. 344–354, 2022, doi: 10.1016/j.matpr.2021.05.447.

[8] M. Minervini, M. E. Mognaschi, P. Di Barba, and L. Frosini, "Convolutional neural networks for automated rolling bearing diagnostics in induction motors based on electromagnetic signals," *Applied Sciences*, vol. 11, no. 17, Aug. 2021, doi: 10.3390/app11177878.

[9] T. A. Dhomad and A. A. Jaber, "Bearing fault diagnosis using motor current signature analysis and the artificial neural network," *International Journal on Advanced Science, Engineering and Information Technology*, vol. 10, no. 1, pp. 70–79, Feb. 2020, doi: 10.18517/ijaseit.10.1.10629.

[10] T. Garcia-Calva, D. Morinigo-Sotelo, V. Fernandez-Cavero, and R. Romero-Troncoso, "Early detection of faults in induction motors—A review," *Energies*, vol. 15, no. 21, Oct. 2022, doi: 10.3390/en15217855.

[11] P. Vas, *Parameter estimation, condition monitoring, and diagnosis of electrical machines*. Oxford University PressOxford, 1992.

[12] N. Bessous, S. Sbaa, and A. C. Megherbi, "Mechanical fault detection in rotating electrical machines using MCSA-FFT and MCSA-DWT techniques," *Bulletin of the Polish Academy of Sciences Technical Sciences*, pp. 571–582, Jun. 2019, doi: 10.24425/bpasts.2019.129655.

[13] Y. Lei, "Fault diagnosis of rotating machinery based on empirical mode decomposition," in *Structural Health Monitoring*, Springer International Publishing, 2017, pp. 259–292.

[14] Y. Li, M. Xu, R. Wang, and W. Huang, "A fault diagnosis scheme for rolling bearing based on local mean decomposition and improved multiscale fuzzy entropy," *Journal of Sound and Vibration*, vol. 360, pp. 277–299, Jan. 2016, doi: 10.1016/j.jsv.2015.09.016.

[15] X. Gu and C. Chen, "Rolling bearing fault signal extraction based on stochastic resonance-based denoising and VMD," *International Journal of Rotating Machinery*, vol. 2017, pp. 1–12, 2017, doi: 10.1155/2017/3595871.

[16] M. Somvanshi, P. Chavan, S. Tambade, and S. V Shinde, "A review of machine learning techniques using decision tree and support vector machine," in *2016 International Conference on Computing Communication Control and automation (ICCUBEA)*, Aug. 2016, pp. 1–7, doi: 10.1109/iccubea.2016.7860040.

[17] J. Li, X. Yao, X. Wang, Q. Yu, and Y. Zhang, "Multiscale local features learning based on BP neural network for rolling bearing intelligent fault diagnosis," *Measurement*, vol. 153, Mar. 2020, doi: 10.1016/j.measurement.2019.107419.

[18] M. K. Saini and A. Aggarwal, "Detection and diagnosis of induction motor bearing faults using multiwavelet transform and naive Bayes classifier," *International Transactions on Electrical Energy Systems*, vol. 28, no. 8, Apr. 2018, doi: 10.1002/etep.2577.

[19] Q. Wang, S. Wang, B. Wei, W. Chen, and Y. Zhang, "Weighted K-NN classification method of bearings fault diagnosis with multi-dimensional sensitive features," *IEEE Access*, vol. 9, pp. 45428–45440, 2021, doi: 10.1109/access.2021.3066489.

[20] P. Kamat *et al.*, "Bearing fault detection using comparative analysis of random forest, ANN, and autoencoder methods," in *Communication and Intelligent Systems*, Springer Singapore, 2021, pp. 157–171.

[21] M. Seera and C. P. Lim, "Online motor fault detection and diagnosis using a hybrid FMM-CART model," *IEEE Transactions on Neural Networks and Learning Systems*, vol. 25, no. 4, pp. 806–812, Apr. 2014, doi: 10.1109/tnnls.2013.2280280.

[22] X. Wang, R. Meng, G. Wang, X. Liu, X. Liu, and D. Lu, "The research on fault diagnosis of rolling bearing based on current signal CNN-SVM," *Measurement Science and Technology*, vol. 34, no. 12, Sep. 2023, doi: 10.1088/1361-6501/acefed.

[23] J. Ma, L. Jiang, S. Li, H. Sheng, C. Zhou, and X. Li, "Fault diagnosis of motor bearing based on current bi-spectrum and convolutional neural network," *Latin American Journal of Solids and Structures*, vol. 20, no. 5, 2023, doi: 10.1590/1679-78257364.

[24] T. Huang, Q. Zhang, X. Tang, S. Zhao, and X. Lu, "A novel fault diagnosis method based on CNN and LSTM and its application in fault diagnosis for complex systems," *Artificial Intelligence Review*, vol. 55, no. 2, pp. 1289–1315, Apr. 2021, doi: 10.1007/s10462-021-09993-z.

[25] D. T. Hoang and H. J. Kang, "A motor current signal-based bearing fault diagnosis using deep learning and information fusion," *IEEE Transactions on Instrumentation and Measurement*, vol. 69, no. 6, pp. 3325–3333, Jun. 2020, doi: 10.1109/tim.2019.2933119.

[26] C. Lessmeier, J. K. Kimotho, D. Zimmer, and W. Sextro, "Condition monitoring of bearing damage in electromechanical drive systems by using motor current signals of electric motors: A benchmark data set for data-driven classification," *PHM Society European Conference*, vol. 3, no. 1, Jul. 2016, doi: 10.36001/phme.2016.v3i1.1577.

BIOGRAPHIES OF AUTHORS

Hai Dang Huu was born in Hai Duong Province, Vietnam. He received Master of Engineering degree in electronic engineering from Le Quy Don Technical University in 2018. He has pursuing his Ph.D. degree with Academy of Military Science and Technology, Hanoi, Vietnam. His research interests include bearing fault diagnosis digital signal processing, machine learning and deep learning. He can be contacted at email: danghai1612@gmail.com.

Ngoc-My Bui was born in Hai Phong City, Vietnam. He received his Ph.D. from Saint Petersburg Electrotechnical University "LETI," Russia, in 2006, majoring in electronic engineering, and became an associate professor in 2018 at the Academy of Military Science and Technology, Hanoi, Vietnam. Currently researching and teaching in the fields of electronics and telecommunications, ultra-high frequency technology, and optical transmission. Electricity, hydroacoustic. He is the author and co-author of more than 48 publications and has two patents. He can be contacted at email: buingocmy_vn@mail.ru.

Van-Phuc Hoang was born in Hung Yen Province, Vietnam. He received Ph.D. degree in electronic engineering from the University of Electro-Communications, Tokyo, Japan in 2012. He has worked as Postdoc researcher, visiting scholar at the University of Electro-Communications, Tokyo, Japan and University of Strathclyde, Glasgow, UK during the period of 2012-2014. He is working as an associate professor, director, Institute of System Integration, Le Quy Don Technical University, Hanoi, Vietnam. His research interests include embedded systems for internet of things, VLSI architecture for digital signal processing, digital circuits and systems, low power IC design and hardware security. He can be contacted at email: phuchv@lqdtu.edu.vn.

Thang Bui Quy was born in Hai Duong, Vietnam. He received his B.S. degree in electronic/electrical engineering in 2009, M.S. degree in cybernetics and automation engineering in 2013 from Le Quy Don Technical University, Hanoi, Vietnam, and Ph.D. degree in computer engineering from University of Ulsan, Ulsan, South Korea, in 2022. He is currently working for Institute of System Integration, Le Quy Don Technical University, Hanoi, Vietnam. His research interests include fault diagnosis and condition monitoring, signal processing, artificial intelligence, system identification, and embedded systems. He can be contacted at email: bqthangcndt@gmail.com.

Yen Hoang Thi received B.S. degree and M.S. degree in electronics engineering from Le Quy Don Technical University, Hanoi, Vietnam, in 2013 and 2019, respectively. Her Ph.D. degree in biomedical engineering was received from The University of Electro-Communications (UEC), Tokyo, Japan in 2023. She got IEEE GCCE Excellent Demo Award in 2022 and Best Student Paper Award at IEEE ATC in 2022. She currently works as a lecturer at Le Quy Don Technical University, Hanoi, Vietnam. Her interests include biomedical engineering, signal processing, deep learning and FPGA-based system design. She can be contacted at email: yenht@lqdtu.edu.vn.